Acta Biomaterialia 9 (2013) 8167–8181

Contents lists available at SciVerse ScienceDirect

Acta Biomaterialia

journal homepage: www.elsevier.com/locate/actabiomat

New biotextiles for tissue engineering: Development, characterization and *in vitro* cellular viability

Lília R. Almeida [a,b], Ana R. Martins [a,b], Emanuel M. Fernandes [a,b], Mariana B Oliveira [a,b], Vitor M. Correlo [a,b], Iva Pashkuleva [a,b], Alexandra P. Marques [a,b], Ana S. Ribeiro [c], Nelson F. Durães [c], Carla J. Silva [c], Graça Bonifácio [d], Rui A. Sousa [a,b], Ana L. Oliveira [a,b,e,*], Rui L. Reis [a,b]

[a] *3B's Research Group – Biomaterials, Biodegradables and Biomimetics, University of Minho, Headquarters of the European Institute of Excellence on Tissue Engineering and Regenerative Medicine, AvePark, 4806-909 Caldas das Taipas, Portugal*
[b] *ICVS/3B's – PT Government Associated Laboratory, Braga/Guimarães, Portugal*
[c] *CeNTI, Centre for Nanotechnology and Smart Materials, V.N. Famalicão, Portugal*
[d] *CITEVE, Technological Centre for Textile and Clothing Industry, V.N. Famalicão, Portugal*
[e] *Department of Health Sciences, Portuguese Catholic University, Viseu, Portugal*

ARTICLE INFO

Article history:
Received 11 February 2013
Received in revised form 20 May 2013
Accepted 22 May 2013
Available online 30 May 2013

Keywords:
Textile
Polybutylene succinate
Silk
Tissue engineering
Biomedical

ABSTRACT

This work proposes biodegradable textile-based structures for tissue engineering applications. We describe the use of two polymers, polybutylene succinate (PBS) proposed as a viable multifilamentand silk fibroin (SF), to produce fibre-based finely tuned porous architectures by weft knitting. PBS is here proposed as a viable extruded multifilament fibre to be processed by a textile-based technology. A comparative study was undertaken using a SF fibre with a similar linear density. The knitted constructs obtained are described in terms of their morphology, mechanical properties, swelling capability, degradation behaviour and cytotoxicity. The weft knitting technology used offers superior control over the scaffold design (e.g. size, shape, porosity and fibre alignment), manufacturing and reproducibility. The presented fibres allow the processing of a very reproducible intra-architectural scaffold geometry which is fully interconnected, thus providing a high surface area for cell attachment and tissue in-growth. The two types of polymer fibre allow the generation of constructs with distinct characteristics in terms of the surface physico-chemistry, mechanical performance and degradation capability, which has an impact on the resulting cell behaviour at the surface of the respective biotextiles. Preliminary cytotoxicity screening showed that both materials can support cell adhesion and proliferation. These results constitute a first validation of the two biotextiles as viable matrices for tissue engineering prior to the development of more complex systems. Given the processing efficacy and versatility of the knitting technology and the interesting structural and surface properties of the proposed polymer fibres it is foreseen that the developed systems could be attractive for the functional engineering of tissues such as skin, ligament, bone or cartilage.

© 2013 Acta Materialia Inc. Published by Elsevier Ltd. All rights reserved.

1. Introduction

The use of fibres and textiles as components of implantable devices is widespread and covers a broad range of applications in medicine and healthcare. Textiles have been successfully used in close contact with complex biological environments as a part of devices such as heart valve sewing rings, vascular grafts, hernia repair meshes and percutaneous access devices [1]. Today, with advances in regenerative medicine, these so-called biotextiles [1,2] offer new possibilities as scaffolds to engineer different biological tissues, thus creating alternatives to harvested tissues, implants and prostheses. Some examples demonstrate the viability of this approach: Moutos et al. [3] designed a biomimetic three-dimensional (3-D) woven composite scaffold for functional tissue engineering of cartilage; Chen et al. [4] developed a new practical ligament scaffold based on the synergistic incorporation of a plain knitted silk structure and a collagen matrix; Liu et al. [5] fabricated a combined scaffold with web-like microporous silk sponges formed in the openings of a knitted silk mesh; Fan et al. [6] rolled a combined silk scaffold around a braided silk cord with mesenchymal stem cells to regenerate the anterior cruciate ligament in a pig model. These few cases reveal the versatility of biotextiles and the rapid advancement in this field.

* Corresponding author at: 3Bs Research Group – Biomaterials, Biodegradables and Biomimetics, University of Minho, Headquarters of the European Institute of Excellence on Tissue Engineering and Regenerative Medicine, AvePark, 4806-909 Caldas das Taipas, Portugal. Tel.: +351 253 510908; fax: +351 253 510909.
E-mail address: analeite@dep.uminho.pt (A.L. Oliveira).

1742-7061/$ - see front matter © 2013 Acta Materialia Inc. Published by Elsevier Ltd. All rights reserved.
http://dx.doi.org/10.1016/j.actbio.2013.05.019

In a typical tissue engineering scenario biomaterial constructs must fulfil certain basic requirements, such as an adequate surface area and chemistry, defined porosity and pore interconnectivity to enable cell adhesion, migration and proliferation and to allow the transport of nutrients and vascularization [7]. Moreover, the construct should be able to restore biomechanical function and maintain controllable degradation during all stages of manipulation, from cell culture to implantation and thereafter. To date several strategies to prepare porous 3-D biodegradable scaffolds for TE have been proposed, with different levels of success. These include gas foaming, fibre extrusion and bonding, phase separation, emulsion freeze-drying, porogen leaching and rapid prototyping [7,8]. Interconnected fibre networks have been demonstrated to be particularly interesting as they provide a high porosity, interconnectivity and surface area [9], which positively influences cell adhesion and proliferation as it resembles the fibrous architecture of the extracellular matrix. Nevertheless, most of these fabrication techniques heavily depend on manual intervention, leading to costly processing procedures which are difficult to reproduce and up scale. Textile technologies are a viable alternative to those approaches, since they allow the production of finely tuned, fibre-based complex constructs with superior control over the design (e.g. size, shape, porosity and fibre alignment), the manufacture and the reproducibility [2,10]. Moreover, they do not involve the use of toxic solvents and allow production on an industrial scale through spinning, weaving, knitting and non-woven technologies [10]. These technologies have recently been applied to develop tissue engineering strategies that seek to restore the biomechanical function of damaged musculo-skeletal tissues [3,11–14]. In general these tissues are particularly difficult to mimic as they are subjected to complex loading patterns that require tissue architectures with preferentially aligned fibre ultrastructures.

In this work we propose a knitting technology to fabricate biodegradable textile matrices from two bio-based polymers, silk fibroin (SF) and polybutylene succinate (PBS). The rational for using this technology is that the knitted textile substrates are known to exhibit better extensibility and compliance compared with other woven substrates, with enhanced porosity/volume, although of limited thickness [15]. A highly ordered arrangement of interlocking loops is typical of these substrates, which determines the mechanical properties of the substrate. Within the knitted structure the pore distribution varies between the fibres and/or yarns from which the knit is comprised. In the literature a few knitted structures of synthetic or biological materials have already been proposed, either alone [16] or in combination with other types of biomaterials/structures to construct functional 3-D scaffolds applicable in the repair/replacement and regeneration of tissues or organs such as vascular [17–19], tendon and ligament [4–6,17,20–22], cartilage [23–25] and skin [26] tissue. As this is a new field of application of knitting technologies most of these applications are still in the exploratory stage.

The idea of studying two structurally different fibres to produce knitted constructs can allow exploration of two markedly different systems in terms of mechanical performance, surface chemistry and degradation profile and, thus, open the possibility of TE applications. PBS is one of the most accessible biodegradable polymers. It is an aliphatic polyester with good processability and flexibility, with degradation products that are non-toxic and which can enter the metabolic cycles of bioorganisms. Besides being extensively studied for its potential use as a conventional plastic [27], it has also been proposed as a support for different approaches in the medical field, alone [28] or in combination with other polymers [29,30]. Correlo et al. [31] reported the production of chitosan-PBS fibre-based structures by melt processing to be used as tissue engineering scaffolds. The raw materials (chitosan and PBS) were compounded and extruded as 400 μm diameter fibres. The approach used to produce the scaffolds was melt compression. To our knowledge this is the first time PBS has been proposed as a viable multifilament fibre (filaments <50 μm) to be processed by a textile-based technology. This particular polymer has advantages compared with other synthetic polymers, such as polylactides (e.g. polylactic acid (PLA) and polyglycolic acid (PGA)), polyethylene oxide (PEO) and poly(lactic acid-co-glycolic acid) (PLGA) [29,30]. Even though they possess certain controllable and reproducible manufacturing characteristics on the large scale, they also have several disadvantages, like the lack of cell recognition signals. Further, specific features of some polymers, such as for example the acidic by-products released during degradation of PLA, present additional difficulties to their use.

SF is a natural biodegradable protein that has been proposed in different forms for several biomedical applications [32–35]. Silk fibres and yarns have extraordinary mechanical properties and have been widely validated over recent years as sutures and textile-based matrices [32,33,36–40]. Horan et al. [32,33] assessed a variety of yarn fabrication techniques, such as plying, twisting, cabling, braiding and texturing, using *Bombyx mori* silk fibres. Recently a number of knitted silk structures have been formulated for the construction of functional 3-D scaffolds for several tissue engineering applications [4–6,17,20,21]. We here use a biodegradable SF textile matrix as a comparative gold standard to validate the knitted PBS matrices. However, since the potential of this natural textile is far from being fully explored new possibilities could emerge as a consequence of the present study.

Development and optimization of the fibres and the respective processing conditions are presented and discussed below. The final developed knitted PBS and silk constructs are screened regarding their morphology, mechanical and surface properties, swelling ability, degradation behaviour and cytotoxicity using a L929 mouse fibroblast cell line.

2. Materials and methods

2.1. Materials

Granulated polybutylene succinate (PBS) was obtained from Showa Highpolymer Co. Ltd (Tokyo, Japan). Silk derived from the silkworm *Bombyx mori* in the form of cocoons was obtained and spun into yarn at the sericulture facility of the Portuguese Association of Parents and Friends of Mentally Disable Citizens.

2.2. Fibre processing and optimization

PBS fibres composed of 36 filaments were processed and optimized in a multicomponent extruder in mono-component mode (Hills Inc., West Melbourne, FL). The melt flow rate (MFR) was determined in order to obtain the adequate processing window. Modular melt flow equipment with an automatic cutter was used according to the standard ASTM D1238. The test was performed at 190 °C with the application of a 2.160 kg force. The results allowed the optimal parameters for the extrusion process (pre-drying of 2 h at 60 °C, thermal profile 120–130 °C, draw ratio 2, speed 300–600 m min^{-1}) to be defined.

2.3. Linear density, tenacity and elongation

The SF and PBS fibres were characterized in terms of linear density, tenacity and elongation. The linear density (tex) is defined as the mass in grams per 1000 m and was determined according to standard EN ISO 2060. The tests were performed using three samples of 10 m each in a conditioned atmosphere at 20 ± 2 °C and 65 ± 4% relative humidity. The tenacity and elongation were mea-

sured according to standard EN ISO 2062. For these tests 250 mm samples were used and 50 replicates were performed. A pre-tension of 0.5 cN tex^{-1} and a velocity of 250 mm min^{-1} were applied in a conditioned atmosphere at 20 ± 2 °C and 65 ± 4% relative humidity.

2.4. Production of the textile constructs

Plain two-dimensional constructs were produced through weft knitting using PBS and raw silk fibres (Tricolab, Sodemat, Germany). The knitted fabrics consisted of consecutive rows of loops, termed stitches. As each row progresses, a new loop is pulled through an existing loop. The active stitches are held on a needle until another loop can be passed through them. In weft knitting the wales are perpendicular to the course of the yarn. This process results in a very stretchy fabric.

All constructs were washed in a 0.15% (w/v) natural soap aqueous solution for 2 h and then rinsed with distilled water. This procedure removed any oil residues due to the fabrication process. In the case of the silk matrices it was also regarded as a preliminary degumming process. *Bombyx mori* silkworm fibres are composed of a core protein called fibroin that is naturally coated with sericin, which is known to be cytotoxic [32,36]. Saponification is a very common degumming process and was used to extract the sericin from the all fibre regions within the textile matrices. Afterwards the silk structures underwent a subsequent degumming process of boiling for 60 min in a 0.03 M Na_2CO_3 solution and rinsing with distilled water to ensure full sericin extraction:

2.5. Morphological characterization

Scanning electron microscopy (SEM) analysis was performed using a Leica Cambridge S360 (UK) to investigate the morphology of the constructs and their cross-sectional structure. The diameters of the fibres were measured and the average of five fibres for each polymer calculated. SEM was used to evaluate any structural changes after degradation studies for different periods (1, 3 and 7 days). All samples were sputter coated with gold (JEOL JFC 1000, UK).

Microcomputed tomography (μCT) (SkyScan, Belgium) was used as a non-destructive technique for a detailed analysis of the 3-D morphology of the textile constructs. Two specimens of each material were scanned in high resolution mode at 3.96 μm $x/y/z$ with an exposure time of 1792 ms. The scanner energy parameters were 63 keV with a current of 157 μA. Isotropic slice data were obtained by the system and reconstructed as two-dimensional images. From these 100 slices were selected and analysed to render 3-D images and obtain quantitative architectural parameters, namely porosity, mean pore size and mean wall thickness. A μCT analyser and a μCT Realistic Volume 3D Visualizer, both from SkyScan, were used as image processing tools for both CT reconstruction and to create/visualize the 3-D representation.

2.6. Mechanical properties

The mechanical properties of the PBS and SF textile constructs were determined by performing quasi-static tensile tests (Instron 4505 Universal, USA). The tensile modulus, ultimate tensile strength and strain at maximum load were measured using a 1 kN load cell at a crosshead speed of 5 mm min^{-1}. The tensile modulus was determined in the most linear region of the stress–strain curve using the secant method.

To investigate the anisotropic behaviour of the constructs tensile tests were performed in the longitudinal (y-axis) and transverse (x-axis) directions of the knitted matrix. Both the dry and hydrated states were studied to determine the effect of the surrounding biological fluids on the mechanical properties of the constructs. The tests performed in the dry state were conducted at 25 °C and 50% humidity. For the hydrated state phosphate-buffered saline, pH 7.4 was used. Samples were immersed for 3 days before testing. Five 15 × 40 mm samples were analysed per condition.

The dynamic mechanical behaviour of PBS and SF constructs was also determined by dynamic mechanical analysis (DMA), using Tritec 2000 DMA equipment (Triton Technology, UK). All tests were carried out in both the dry and hydrated states, at 37 °C and in the longitudinal direction. For the measurements performed in the hydrated state samples were immersed in a phosphate-buffer saline solution for 3 days before testing to ensure complete hydration. The test was performed in solution using a chamber specific for the purpose. The samples were subjected to three tensile cycles at increasing frequencies ranging from 0.1 to 10 Hz with constant amplitude displacements of 0.03 mm. Both the storage modulus (E') and loss factor ($\tan\delta$) were obtained in the frequency range. All textile membranes were accurately measured and at least five specimens were tested per condition.

2.7. Surface characterization

Surface characterization is extremely important in understanding the response of cells to the materials,. For proper surface characterization we prepared PBS and SF membranes and related the results obtained to the real scenario, i.e. the surface of the fibres. PBS membranes were produced by melt-compression of granules. SF membranes were cast from a water-based SF solution, prepared as previously described by Yan et al. [41]. Briefly, the cocoons were consecutively boiled in an aqueous solution of 0.02 M sodium carbonate for 60 min and in 0.01 M sodium carbonate for 30 min. The extracted SF was washed with distilled water. After drying at 60 °C the SF (20% w/v) was dissolved in 9.3 M LiBr solution at 70 °C for 1 h. This solution was dialysed for 3 days. SF membranes were obtained by casting the solution in a Petri dish and slow drying at room temperature. In order to induce a β-sheet conformation the membranes were immersed in a series of methanol/water solutions with increasing concentrations of methanol up to 100%. Ideally it would be preferable to produce a membrane through self-assembly as a way to recreate the natural process of SF fibre formation and mimic the natural silk structure, however these processes remain poorly understood, which makes the reconstitution of silk solutions into materials with properties comparable with the native state problematical [42]. Therefore, we decided to induce β-sheet formation through methanol treatment in order to achieve reproducible surfaces that were comparable with those found in the native SF fibres.

The surface chemistry of the membranes was analysed by Fourier transform infrared attenuated total reflectance (FTIR-ATR) spectroscopy, contact angle measurements and X-ray photoelectron spectroscopy (XPS).

FTIR spectroscopy is a powerful method to examine protein structure as well as conformation transition processes. In this particular study this technique was used to illustrate the different chemical nature of each polymer. FTIR spectra were recorded in an IR Prestige 21 (Shimadzu, Germany) spectroscope with an attenuated total reflectance (ATR) device. Spectra were obtained in the wavelength range 800–4000 cm^{-1} with a resolution of 4 cm^{-1}.

Understanding the surface behaviour of a biomaterial in contact with a hydrated medium is of importance in predicting the interactions of a material with the surrounding tissues when used in a particular biomedical application. The wettability of the surfaces was assessed by contact angle (θ) measurements. Static contact angle measurements were obtained by the sessile drop method using

an OCA15+ contact angle meter with a high performance image processing system (DataPhysics Instruments, Germany). The surface energies of the membranes produced from each material were evaluated using two liquids, H_2O and CH_2I_2 (1 μl, HPLC grade), added using a motor driven syringe at room temperaturs. Two samples of each material were used and five measurements were carried out per sample. The surface free energy (γ) of the samples was calculated by the Owens, Wendt, Rabel and Kaelble (OWRK) method [43,44]. XPS was also used to characterize the surface elemental composition of PBS and silk membranes.

XPS is one of the most effective spectroscopic techniques available for surface analysis of polymers, and has many advantages for studying biomaterials. These include a high sensitivity to surface variations, the high speed of analysis, the high information content, little damage to the sample, and the ability to analyse samples without specimen preparation. The XPS analyses were performed using a Thermo Scientific K-Alpha ESCA instrument. Monochromatic AlK_α radiation from a 1486.6 eV X-ray source and a take-off angle of 90° relative to the sample surface were used. The measurements were perfomed in constant analyser energy (CAE) mode with 100 eV pass energy for survey spectra and 20 eV pass energy for high resolution spectra. Charge referencing was adjusted by setting the binding energy of the hydrocarbon C1s peak at 285.0 eV. Overlapping peaks were resolved into their individual components using XPSPEAK 4.1 software.

2.8. Degradation studies

The degree of hydration and degradation behaviour of the SF and PBS textile constructs were studied in vitro. Both polymers are known to be sensitive to certain enzymes present in the human body. PBS constructs (n = 4, weight ~90 mg each) were immersed in 4 ml of a phosphate-buffered saline solution (0.01 M, pH 7.4) containing 0.01 mg lipase ml $^{-1}$ (150 U l^{-1}) from *Pseudomonas cepacia* (Sigma, 15 U/mg) U mg^{-1}) [45]. The serum lipase concentration in healthy adults is in the range 30–190 U l^{-1}. The SF constructs (n = 4, weight ~65 mg each) were immersed in 4 ml of phosphate-buffered saline solution containing 1.0 mg protease XIV ml^{-1} (3500 U l^{-1}). Protease XIV was derived from *Streptomyces griseus* (Sigma, 3.5 U mg^{-1}) [46]. Both the lipase and protease concentrations are in the range of values found in the human body [45,46]. As a control samples were incubated in PBS alone. The study was conducted at 37 °C for periods of 1, 3, 7, 14 and 30 days, under sterile conditions. The solutions were changed weekly. At the end of each period the samples were removed from the solution, washed, gently blotted with a filter paper to remove excess liquid and weighed. The pH of each solution was also monitored. The weight loss was determined as:

$$\text{weight loss}(\%) = [(m_i - m_d)/m_i] \times 100 \quad (1)$$

where m_i is the initial weight of the sample and m_d is the weight of the sample after drying. The percentage hydration was calculated as:

$$\text{degree of hydration}(\%) = [(m_w - m_f)/m_f] \times 100 \quad (2)$$

where m_w is the weight of the sample after removal from the solution and m_f is the weight of the sample after drying. The values obtained are presented as averages ± standard deviation and are plotted as function of time.

2.9. Thermal properties

The differential scanning calorimetry (DSC) experiments were performed in a TA Instrument model DSC Q100 (USA), under a nitrogen atmosphere as purge gas (gas flux ~50 ml min^{-1}). The samples were scanned in two continuous thermal cycles at the rate of 10 °C min^{-1}, from −20 to 150 °C for PBS and up to 350 °C for SF. In the case of SF textiles the first cycle from −20 to 140 °C was used to remove any water. Two samples with a mass of 5.5–6 mg for PBS and 2.5–3 mg for SF were used per condition. The thermograms of the second thermal cycle and of the first cooling cycle were used for analysis. The degree of crystallinity was calculated using the equation:

$$\text{degree of crystallinity}(\%) = (\Delta H_m/\Delta H^0) \times 100 \quad (3)$$

where ΔH_m is the melting enthalpy of the polymer and ΔH^0 is the enthalpy of 100% crystalline PBS (H^0 = 110.3 J g^{-1}) [47].

2.10. Cell culture

The materials were cut into discs with a diameter of 16 mm, placed in 24-well culture plates (BD Biosciences, USA) and immobilized on the bottom of each well using CellCrown® inserts (Scaffdex, Finland). Mouse fibroblastic cells (L929, ECACC, UK) were seeded onto the materials at a concentration of 1×10^4 cells per sample and cultured at 37 °C, 5% CO_2 and 95% humidity in Dulbecco's modified Eagle's medium (DMEM) (Sigma Aldrich, Germany) with phenol red, supplemented with 10% foetal bovine serum (FBS) (Biochrom, Germany) and 1% antibiotic–antimycotic (Gibco, UK), for 1, 7 and 14 days. The medium was changed every 2–3 days. Tissue culture polystyrene (TCPS) (Sarstedt, USA) coverslips were used as a control.

2.11. Scanning electron and optical microscopy

Cell adhesion and morphology were analysed by SEM and by optical microscopy after methylene blue staining. After each incubation time materials were washed with PBS (Sigma, USA), fixed with 2.5% glutaraldehyde (Sigma, USA) for 30 min and kept at 4 °C in buffer until preparation for staining and SEM observation. For the methylene blue (Sigma Aldrich, Germany) staining the materials were dipped in a 0.5% methylene blue solution and washed in buffer three times. Samples were analysed with an axioimager Z1 M microscope (Carl Zeiss, Germany) and images were acquired and treated with AxioVision V.4.8 softwear. Prior to SEM analysis the samples were twice dehydrated in graded ethanol solutions (30, 50, 60, 70, 80, 90 and 100 vol.%) for 15 min at each concentration and then in hexamethylidisilazane (HMDS) (Electron Microscopy Sciences, USA). Samples were mounted on metal stubs and sputter-coated with gold prior to analysis using a Leica Cambridge S360 scanning electron microscope.

2.12. DNA quantification

The DNA quantification test was conducted in order to assess cell proliferation over the period of culture. After each time point samples were carefully rinsed twice with PBS, immersed in ultrapure water to induce osmotic shock and frozen at –80 °C for subsequent thermal shock. DNA was quantified using the PicoGreen quantification kit (Invitrogen Corp., USA), according to the manufacturer's instructions. To exclude the possibility of material autofluorescence samples without cells were subjected to the same procedure. Fluorescence was read in a microplate reader (BioTek, USA) at 485 excitation and 525 emission.

2.13. Statistical analysis

All numerical data are presented as averages and standard deviations. Statistical analysis was performed for the static mechanical tests and DNA quantification. One way analysis of variance (ANOVA) was used. The comparison between two average values was

performed using Tukey's test with $p < 0.05$ indicating statistical significance.

3. Results and discussion

3.1. Fibre characterization

The applied textile processing methodology is highly demanding in terms of the mechanical properties of the fibres and filaments used. Therefore, it is extremely important that they have an adequate linear density and resistance to degradation. The linear density, resistance to degradationand elongation of the fibres produced are presented in Table 1.

The linear density of PBS fibres was designed to match the value obtained for the silk fibres (77.4 tex) so that both systems would be comparable after knitting. Although PBS fibres had a lower specific strength to rupture both fibres presented mechanical properties in the processing window that allowed effective knitting of textile matrices. The elongation values obtained for PBS fibres were considerably higher, demonstrating its greater capacity for deformation.

DSC analysis was performed for PBS granules (PBS raw) and fibres to investigate possible thermal degradation induced during fibre extrusion. Fig. 1 compares the normalized DSC thermograms for the PBS raw (granulated) with those for the extruded PBS fibres.

During melting of the pure PBS two endothermic peaks were observed, a small one with a maximum at T_m = 102 °C and a large one at T_m = 112.6 °C, which is associated with melting of semicrystalline PBS [48]. The first heating reflects the influence of the processing conditions. The pure PBS had a degree of crystallinity of 65% (Eq. (3)), while a value of 71.4% was determined for the PBS fibres. The higher degree of crystallinity of the fibre can be attributed to the induced orientation of PBS segments during the extrusion process. After the first thermal cycle (removal of the thermal history) non-isothermal crystallization of the PBS fibres indicates that the polymer starts to crystalize at a lower temperature (T_c = 82.5 °C) in the case of PBS fibres compared with pure PBS (T_c = 84.9 °C). The second heating cycle demonstrates similar behaviours for the pure PBS and the fibres consisting of melting, recrystallization and remelting. These results indicate that no degradation takes place during the extrusion process.

Table 1
Linear density (tex), resistance to degradation (c*N*/tex) and elongation (%) of the monocomponent PBS and raw silk fibres.

	Monocomponent fibres PBS	Raw silk fibres
Linear density (tex)	77.3	77.4
Tenacity (cN tex^{-1})	15.2	45
Elongation (%)	120	30

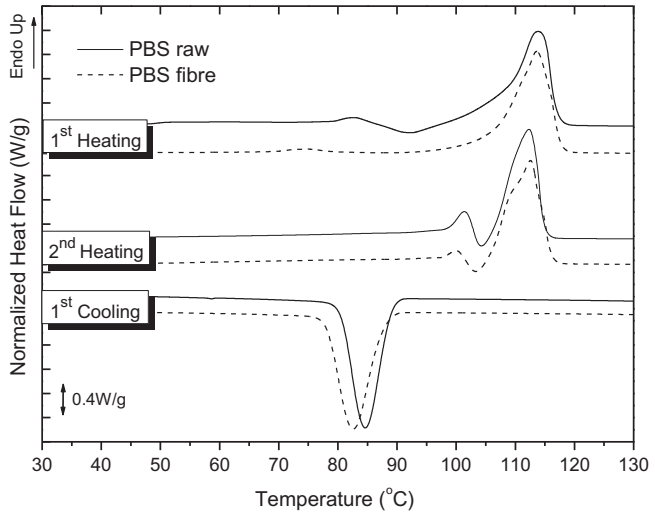


Fig. 1. DSC thermograms for raw PBS (granulated) and PBS fibres (after extrusion) obtained at a scan rate of 10 °C min^{-1}.

3.2. Morphological characterization

Fig. 2 presents details of the morphology of the obtained knitted PBS and SF constructs.

Both matrices present very regular and well-controlled patterns with similar morphologies. The PBS fibres (Fig. 2a) consist of filaments with a circular cross-section having an average diameter of 48.9 ± 0.3 μm. In the case of silk (Fig. 2e) the filaments show an irregular cross-section, typical of this natural fibre, with a lower average cross-section of 9.1 ± 2.2 μm. The number of filaments, however, is much higher for SF than for PBS. Therefore, although both fibres have the same linear density they are structurally different, as their filaments differ in number and size. SF filaments are thinner and in higher number, which could explain the lower pore size due to greater compactation and, consequently, low porosity. Moreover, in the SF matrices some filaments of the fibres are loose in the textile structure due to a degree of physical wear during the degumming process to eliminate sericin. The measured thickness of the PBS matrix was ~0.7 mm, while the silk matrix was ~0.8 mm thick.

In general both constructs (PBS and SF) present a relatively high porosity and an interconnectivity of 100%, meaning that all of the pores are interconnected, as is observable in Fig. 2. The calculated average porosity, mean wall thickness and mean pore size are presented in Table 2.

Although the same fibre linear densities and processing parameters were used to build both knitted structures, the SF matrices had a significantly lower porosity (68.4 ± 3.7 for SF, 78.4 ± 2.3 for PBS) and pore size than of those of PBS (54.5 ± 9.4 for SF, 72.4 ± 13.0 for PBS). These differences can be related to the differences in the respective filament thicknesses. In fact, silk fibres present a higher volume compared with those of PBS) due to the spaces generated between the filaments (as observed in Fig. 2f and g), resulting in a lower interloop space after knitting. The mean pore sizes of both the SF and PBS) matrices are suitable for tissue engineering applications [49]. Considering skin regeneration and wound healing, for example, a study by O'Brien et al. [50] has shown that the critical pore size range of collagen-based scaffolds allowing optimal cellular activity and simultaneous blocking of wound contraction was between 20 and 120 μm. In the case of bone tissue engineering the minimal pore size is considered to be ~75–100 μm [49]. This is due to cell size and cell migration and nutrient/oxygen transport requirements. This pore size has also been associated with the capability for vascularization. Using the present knitting technology it is possible to precisely adjust the interloop space of the textile matrices so that the final porosity (and pore size) can be tailored according to the specific need.

3.3. Mechanical properties

The mechanical properties of the textile constructs were investigated by performing quasi-static tensile tests and DMA analysis. Fig. 3 shows the mechanical behaviours of both the PBS and SF textile constructs.

In the dry state, when comparing both structures in the longitudinal direction (*y*-axis), the average tensile modulus of the PBS matrices (~7.9 MPa) is significantly lower than that determined for SF (31.6 MPa). Accordingly, the corresponding maximum

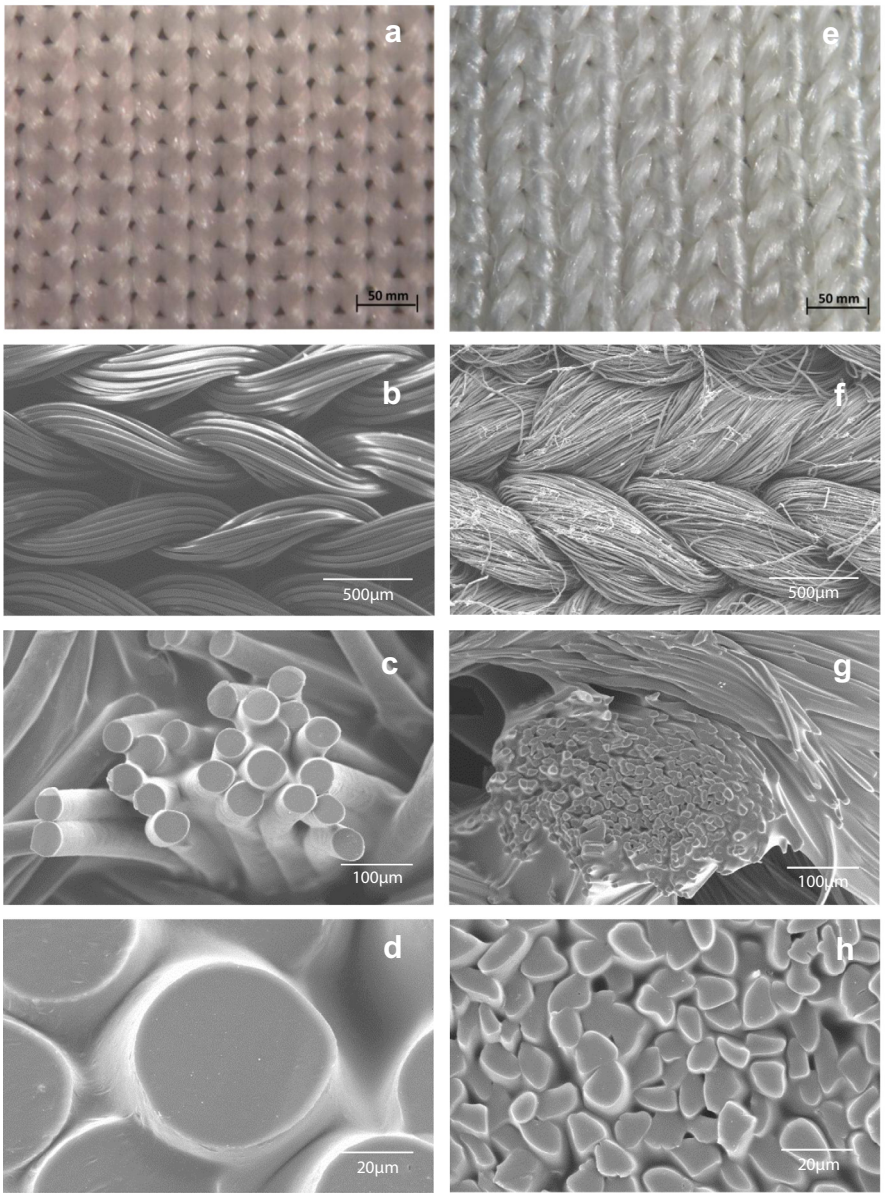


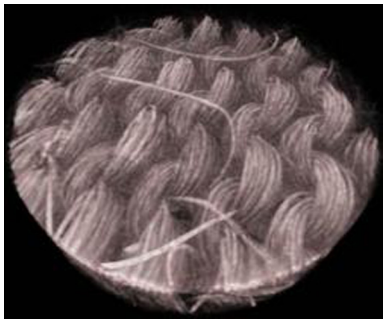
Fig. 2. Morphology of (a–d) PBS and (e–h) SF knitted constructs showing different levels of detail. (a, e) Macroscopic images and (b, f) SEM micrographs showing the top view and (c, d, g, h) the respective fibre cross-sections.

strength for PBS (8.2 MPa) is also lower than that for SF (17.4 MPa). As expected, SF matrices presented a considerable higher strength and stiffness compared with PBS. SF fibres are known for their extraordinary mechanical properties that rival most high performance synthetic fibres. This behaviour is a results of their unique molecular structure and protein conformation [32]. On the other hand, PBS matrices had a higher percentage elongation (155.8%) compared with SF (126.8%), which is in accord with the values obtained for the elongation of single fibres (Table 1). When testing the mechanical properties of the textiles in the transverse direction in the dry state the modulus and maximum strength decreased to 4.4 and 2.8 MPa for PBS and to 11.6 and 8.0 MPa in the case of SF. The same behaviour was observed for PBS matrices, and is independent of the hydration state. This decrease is associated with the anisotropic character of the knitted matrices, which have better mechanical properties in the longitudinal direction compared with the transverse. This property is particularly interesting considering that most tissues have a high degree of anisotropy. For example, in a study by Williams et al. [51] the cancellous bone of the proximal tibial epiphysis had a longitudinal modulus of 129.07 ± 49.48 MPa and a transverse modulus of 38.23 ± 20.18 MPa.

The intrinsic properties of the fibre can also contribute to an increase in the final anisotropy of the textile construct, as demonstrated in the case of the SF textiles as a greater variation in the modulus and maximum strength when changing the direction. SF fibres are secreted in the β-pleated sheet conformation, with the longest axis aligned with the fibre axis. Thus the strength along the fibres results from extended covalent peptide chains. This will contribute to the increased strength and stiffness of the knitted matrices along the longitudinal direction. Loose associations between sheets allow flexibility in the fibre and are also responsible for some ductility [52].

When analysing the mechanical performance in the hydrated state compared with the dry state it can be observed that SF constructs are more affected than PBS constructs. In the case of PBS matrices immersion in a buffer solution resulted in a slight increase in the modulus and maximum strength of the structures

Table 2
3-D reconstructions, average porosity, interconnectivity and mean pore size, calculated from the μCT data.

Material	3-D reconstruction	Porosity (%)	Mean wall thickness (μm)	Mean pore size (μm)
Silk		68.4 ± 3.7	37.8 ± 14.9	54.5 ± 9.4
PBS		78.4 ± 2.3	28.7 ± 5.5	72.4 ± 13.0

when tested in both directions without, however, statistical significance. On the other hand, a significant decrease in the modulus of the SF structures was observed for both the longitudinal and transverse directions.

Fig. 4 shows the storage modulus (E') and loss factor (tan δ) as a function of frequency for samples tested under tension in the longitudinal direction for both the dry and hydrated conditions.

As expected, the storage modulus (E') of the SF constructs was higher, in both the dry and wet states, than the E' of PBS, indicating a higher stiffness of this material (Fig. 4a and b). Under hydrated conditions the SF structures showed a slight decrease in E' value compared with the dry state. This result is consistent with the obtained E values from the static mechanical analysis under similar conditions (Fig. 3) and is related to the effect of water molecules incorporated in the structure of SF fibres, as reported by Perez-Rigueiro et al. [53]. β-sheet platelets in silkworm silk constitute around 50-60% of the total volume of the fibre [52]. It is accepted that this crystalline domain is not affected by water molecules. Thus the observed changes in the elastic moduli of samples tested in air and in buffer solution can be attributed to changes in the amorphous regions. Immersion in water disrupts the hydrogen bonds between chain segments in the amorphous phase, resulting in van der Waals bonds dominating, thus reducing the initial modulus. This will contribute to softening of the structure, which will lead to an increase in ductility, as can be observed in the transverse direction as an increase in the percentage elongation at break. An increase in the E' value of SF, from 25 to 35 Mpa, was observed with the increase in frequency, which may be explained by the sensitiveness of silk to mechanical stimuli, reported to align the polymeric structure and induce the formation of β-sheet structures [52]. PBS constructs showed the opposite behaviour to SF. A higher E' value was observed for samples measured in the hydrated state. This tendency is again in agreement with the E values calculated from the tensile tests (Fig. 3) and may be explained by a release of plasticizers from the PBS structure after 3 days immersion, leading to an increase in stiffness. Also, as reported by Taniguchi et al. [45] some initial degradation could have taken place by preferential hydrolysis of the amorphous regions of the polymer, leading to a decrease in ductility. This effect is consistent with a decrease in the percentage elongation at break.

The loss factor is an important parameter as it will determine the capability of the material to absorb mechanical energy when the implant is subjected to periodic loads at frequencies of about 1 Hz. Silk membranes, in both the dry and hydrated states, showed a higher loss factor than PBS membranes (Fig. 4c and d), i.e. a higher capability of absorbing mechanical energy. This is an interesting feature in a tissue engineering application such as bone, which is subjected to periodic loads. In both cases wetting of the samples led to a decrease in loss factor values, so the structures show a more elastic behaviour under these conditions, rather than a viscous/dissipating behaviour. Initial values of 0.2 for the knitted SF constructs show their viscoelastic character. Viscoelasticity is a characteristic property of natural bone, which has been shown to become stiffer at higher strain rates. For the PBS constructs in the dry state the loss factor remained stable (Fig. 4c). In the wet state an increase in frequency induces a decrease in the loss factor for these constructs, indicating an increase in elastic behaviour with increasing frequency. For SF the loss factor is much less affected by the presence of water in the structure, as can be observed in Fig. 4d. In this case a slight decrease occurs in the dry state for frequencies higher than 1 Hz, while the opposite effect is observed in the wet state, i.e. an increase in the ability to dissipate energy (a more viscous behaviour).

3.4. Surface characterization

Characterization of the surface of the PBS and SF fibres was indirect, through the analysis of membranes of both materials. The FTIR and XPS spectra of the materials under studied are presented in Fig. 5.

Using FTIR it is possible to confirm the different chemical natures of each polymer, which will consequently translate into a

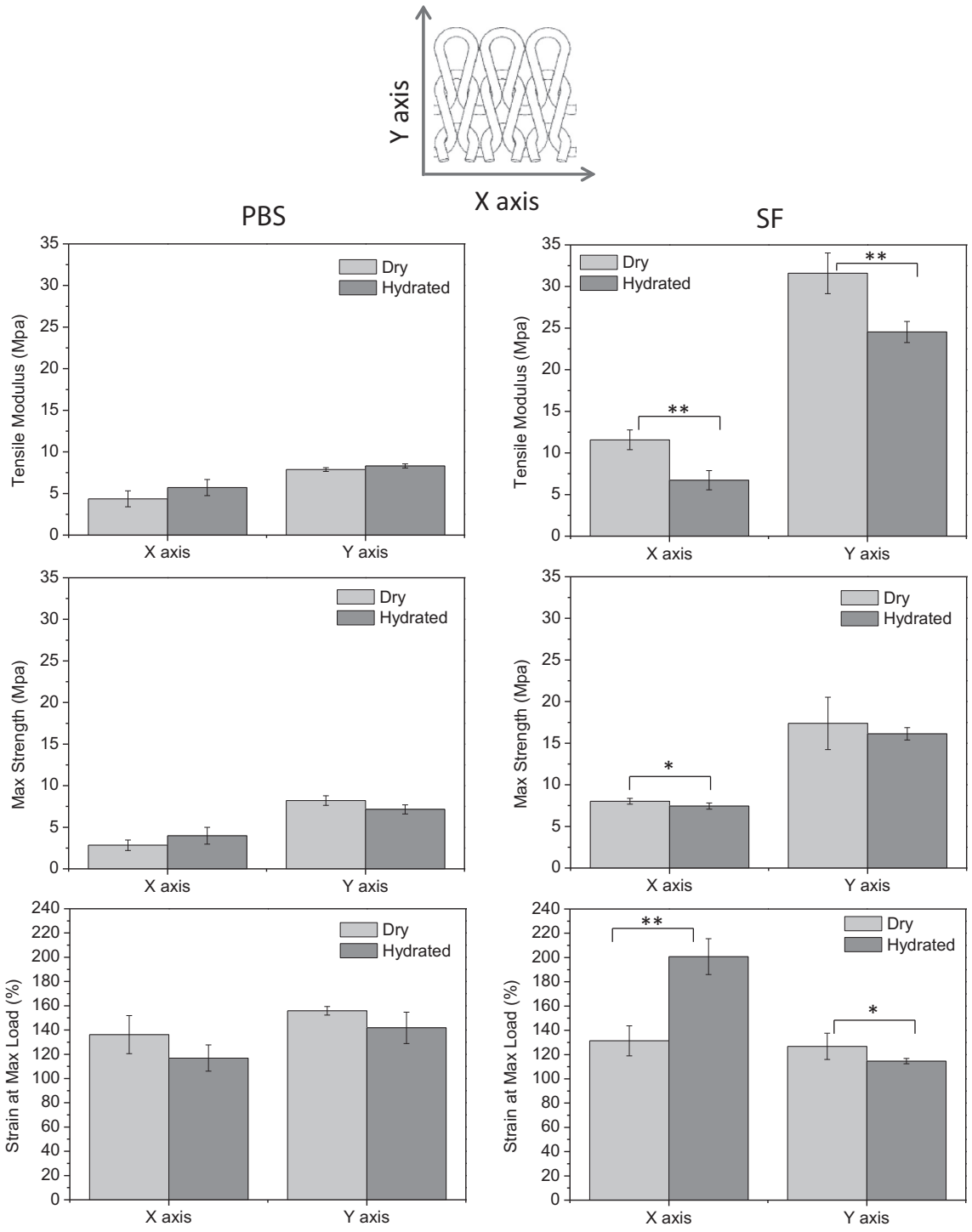


Fig. 3. Maximum strength (MPa), elastic modulus (MPa) and strain at maximum load (%) obtained for SF and PBS samples in the dry (25 °C) and hydrated states (isotonic phosphate buffer solution, 37 °C), in the transverse (*x*-axis) and longitudinal (*y*-axis) directions ($^{*}p < 0.05$; $^{**}p < 0.001$).

quite different surface behaviours. The PBS spectrum shows typical bands for an aliphatic polyester around 1710 cm^{-1}, caused by C=O stretching, and 1160 cm^{-1}, caused by C–O stretching [54,55]. The silk spectrum shows intense bands at 1615 and 1510 cm^{-1}, typical of amide I and amide II, respectively. These two bands indicate the crystalline structure of silk fibroin films by comparison with the spectra before methanol treatment (amide I peak observed at 1652 cm^{-1}, data not shown) [35]. Two amide II vibrations can be observed at 1230 and 1260 cm^{-1}[34,56]. Since FTIR is insufficiently surface sensitive to demonstrate differences between the bulk and surface composition, contact angle and XPS measurements were also performed to complement the surface chemistry information (Fig. 5 and Table 3).

The aliphatic chain confers a hydrophobic character to PBS with a contact angle of 105.7° and a surface energy of 22.3 mN m^{-2}, as can be seen in Table 3. A lower contact angle (66.9°) and higher surface energy (42 mN m^{-2}) were obtained for silk. The XPS data for PBS and SF show the presence of two main elements, C and O (Table 3). As expected, the XPS analysis of SF also demonstrated the presence of a third element, N. The C1s core level signals of

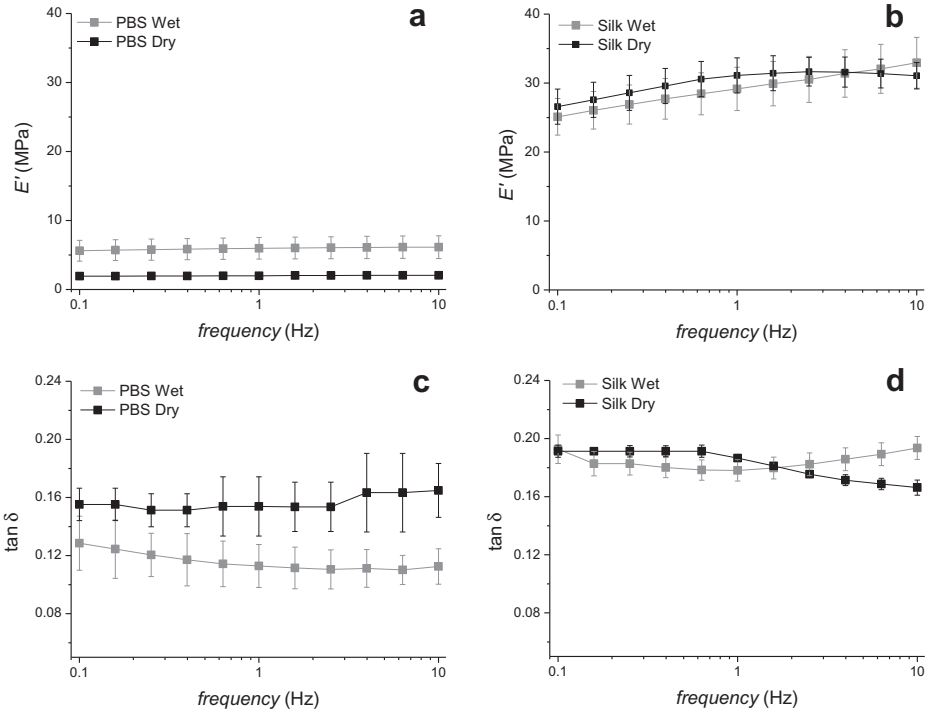


Fig. 4. Storage modulus (E') and loss factor (tan δ) vs. frequency (Hz) tested under tension in the longitudinal direction for (a, c) PBS and (b, d) SF in the dry and hydrated (phosphate buffer, 37 °C) state after 3 days immersion.

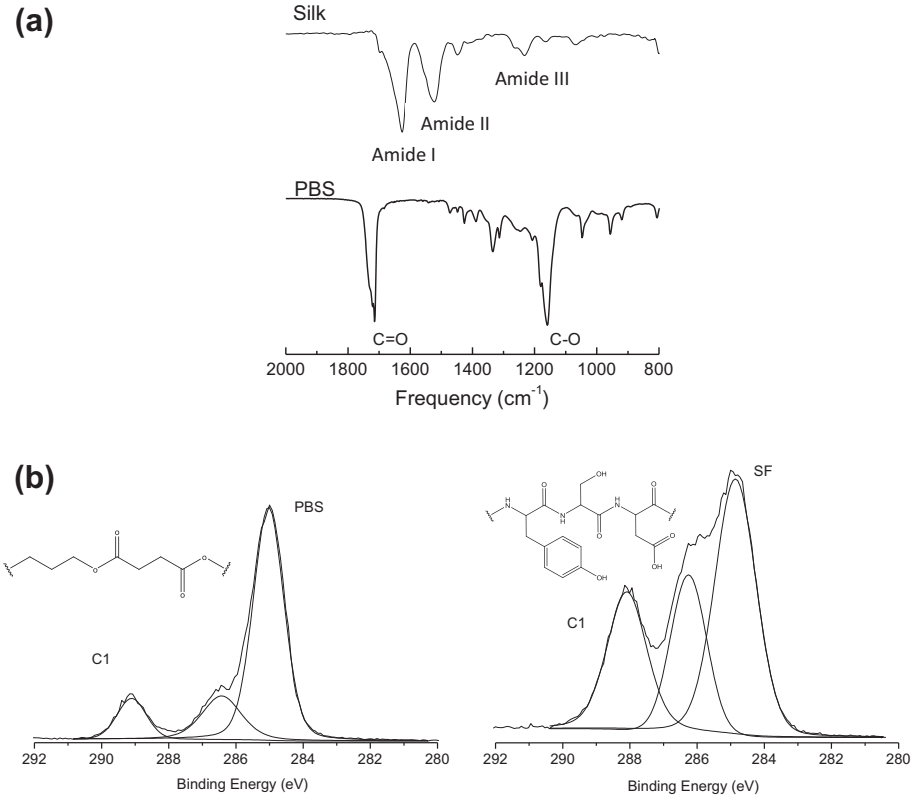


Fig. 5. (a) FTIR spectra and (b) XPS C1s spectra of PBS and SF membranes.

both polymers (Fig. 5) were deconvoluted to three peaks: at 285.0 eV. assigned to C–H/C–C chemical bonds; the peak at 286.4 eV, corresponding to C–O– bonds; a third peak that was different for PBS (at 289.1 eV, assigned to the ester bonds O–C=O) and SF (at 288.34 eV, assigned to the N–C=O bonds of the amide groups). The relative intensities of the last two peaks, associated

Table 3
Water contact angle (θ), surface energy values and surface elemental composition of PBS and SF.

Material	θ	Surface energy (mN m^{-1})			Elemental composition (%)			O:C ratio
		γ_s	γ_s^p	γ_s^d	O	C	N	
PBS	105.7 ± 1.8	22.3	0.2	22.1	17.9	78.8		0.23
SF	57.3 ± 3.3	45.3	19.7	25.7	19.6	63.5	14.9	0.31

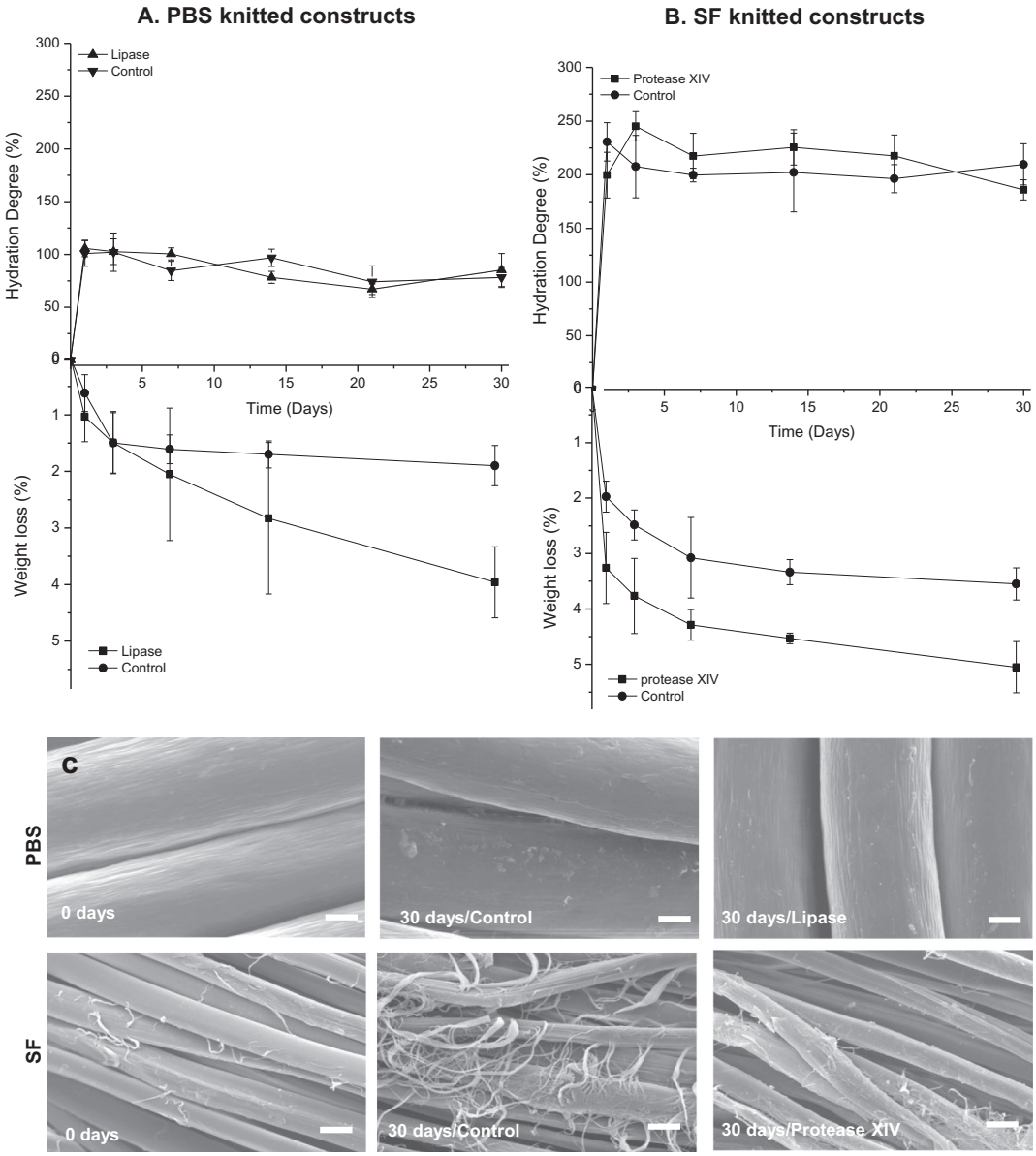


Fig. 6. Degree of hydration and degradation behaviour of (a) PBS and (b) SF knitted constructs after immersion in buffer solution with and without enzyme for up to 30 days (% weight). (c) SEM micrographs of PBS and SF fibres before and after the 30 day degradation study. Scale bar 10 μm.

with the presence of polar groups, demonstrated that they are present at higher concentrations on the surface of SF compared with PBS. Those results are in agreement with both the FTIR-ATR spectra and contact angle measurements.

3.5. Degradation studies

After implantation biomaterials interact with the surrounding environment by absorbing fluids, which have an effect on the material properties, causing dimensional changes. In Fig. 6 the degree of hydration and degradation behaviour are plotted for PBS (Fig. 6a) and SF (Fig. 6b) after immersion in buffer solution with and without enzyme up to 30 days. SEM micrographs of PBS and SF fibres are also presented before and after the 30 day degradation studies (Fig. 6c).

PBS textile constructs reached equilibrium hydration after 3 days, being able to uptake ~100 wt.%. After the same period SF uptook between 200 and 250 wt.%. The capacity for hydration of the proposed knitted constructs results from the combined effect of the surface and bulk properties. The capillarity effect is a well-

known phenomenon which is dependent on the surface wettability [57]. Therefore, since PBS is a hydrophobic polymer the hydration capacity is more related to the capillarity effect than with the ability to take up water into its structure. SF is more hydrophilic than PBS and it is expected that the corresponding knitted structure could take up greater amounts of water. In fact, the results of the mechanical tests demonstrate that water molecules are able to penetrate the SF bulk, decreasing its elastic modulus (Fig. 3 and 4). Another explanation is related to the higher surface area in the case of the SF fibres, due to the lower diameter/higher number of filaments compared with PBS.

According to the literature the degradation of polymeric materials in the living environment can be the result of either enzymatically or chemically induced cleavage, involving water, enzymes, metabolites and ions that interact with the material. Both of the knitted constructs showed relatively small weight losses when immersed in buffer solution without enzyme (control). After 3 days immersion the PBS constructs lost around 1.5% in weight. This initial loss can be related to the release of traces of polymer of low molecular weight, which corroborates the increase in stiffness observed during mechanical testing after the same period of immersion (Figs. 3 and 4), combined with a degree of hydrolytic degradation that occurs in the presence of phosphate buffer, as reported by Chang et al. [28]. SF constructs showed a weight loss of around 3%, most of which occurred in the first week of immersion. Horan et al. [58] studied the in vitro degradation of native silk fibroin yarns over 42 days in a similar buffer solution. The masses of the silk matrices remained unchanged. In our particular case we attribute the weight loss to the release of some fibres from the structure as a result of the degumming process.

The presence of enzyme in the buffer solution did not significantly affect the hydration profile of the constructs. However, the degradation rate increased in both cases. For PBS the weight loss increased to about 4%. Lipase is present in the human body in small concentrations and can be involved in the biodegradation of this synthetic polymer [59]. Polyester biomaterials can be enzymatically degraded by lipase, which catalyse the hydrolysis of ester bonds [45]. On the other hand, silk can be degraded by specific proteases in the human body, for instance those produced by cells involved in the healing response, which are intended to degrade the extracellular matrix around them [60]. As expected, the degradation rate of SF increased to around 5% in the presence of protease XIV. Li et al. [61] detected free amino acids after incubation of silk films in protease XIV solution, demonstrating its potential to cleave silk non-discriminately (i.e. at multiple locations along the length of the protein), supporting the use of this particular protease in this study. Horan et al. [58] also used this type of protease. They changed the solution on a daily basis due to a significant loss in activity when incubated at 37 °C for periods longer than 24 h. In our case the solution was changed weekly, which could be the reason for a lower degradation rate compared with the literature [58]. The morphology of the fibres before and after degradation did not alter

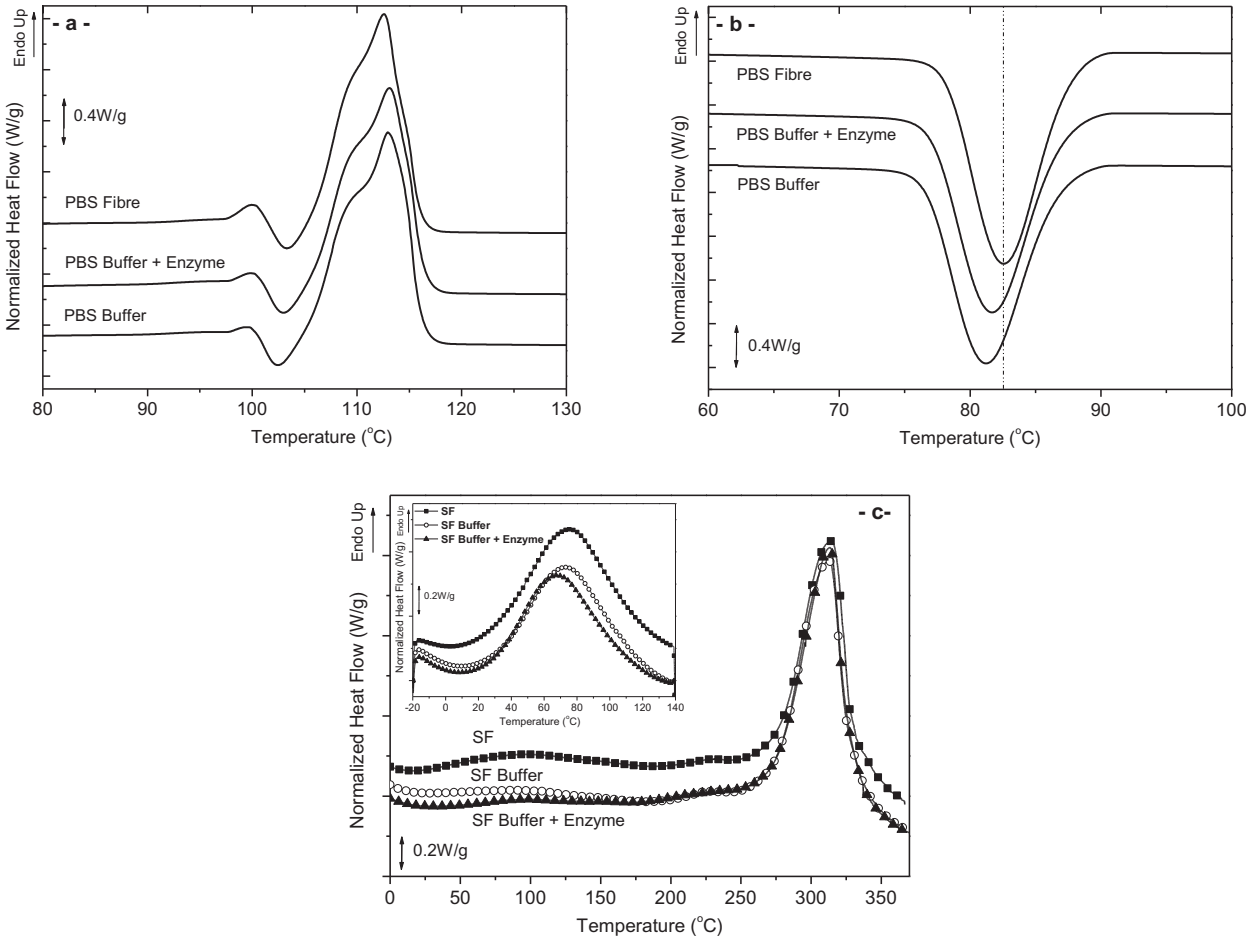


Fig. 7. DSC thermograms for PBS showing (a) the second heating cycle and (b) the first cooling cycle before degradation (PBS fibre) incubated with the phosphate buffer solution and with this solution containing lipase. (c) DSC thermograms for SF textiles: ■, before the degradation study; (○) after incubation in the buffer solution; ▲, after incubation in the buffer solution containing protease.

Table 4
Melting temperature, enthalpy, crystallization temperature and degree of crystallinity of the raw PBS material and after extrusion and degradation.

Sample	T_c[a] (°C)	$T_{c\ (onset)}$[a] (°C)	ΔH_c[a] (J g^{-1})	T_m[b] (°C)	$T_{m\ (onset)}$[b] (°C)	ΔH_m[b] (J g^{-1})	x_c[c] (%)
Raw PBS	62.4	66.5	53.6	92.8	86.0	54.0	48.9
PBS fibre	82.5	87.6	74.9	112.6	105.8	70.2	63.6
PBS	81.4	87.0	75.8	113.0	105.5	74.6	67.7
PBS + lipase	81.7	87.1	75.5	113.0	105.6	74.6	67.6

[a] Maximum crystallization temperature, onset temperature and enthalpy at first cooling from the melt at 10 °C mm^{-1}.
[b] Melting temperature, onset temperature and enthalpy determined by DSC on second heating at 10 °C mm^{-1}.
[c] Degree of crystallinity calculated on the basis of a ΔH^0 value of 110.3 J g^{-1} for 100% crystalline PBS [30,43].

significantly for PBS, while for silk some surface wear was visible (Fig. 6c).

The degree of crystallinity can greatly affect degradation. Therefore, the thermal properties of the knitted constructs before and after 30 days degradation were evaluated by DSC analysis (Fig. 7 and Table 4).

A slight decrease in the crystallization temperature was observed for PBS after immersion in buffer solution for 30 days. Consequently, a slight increase in the degree of crystallinity occurred. This increase can be related to preferential degradation of the amorphous domains of the polymer. Thermograms of the SF textile fibres from the second heating cycle are compared in Fig. 7c. The inset graph shows the first thermal cycle used to remove water from all the samples, which shows a large endotherm signal. It was observed that the non-degraded SF textiles had a higher moisture content compared with the samples submitted to degradation. A large endotherm with a maximum at 313–314 °C was also observed for all samples, and was attributed to the thermal degradation of SF. This result is in accordance with similar SF fibres reported in the literature [62].

3.6. Cell behaviour

The presence of potential oil contamination as a result of the material processing, still present after washing the constructs, was one of our main concerns regarding cytotoxicity. Additionally, the presence of sericin residues in the silk could also lead to some degree of cell death. Therefore, we tested the developed constructs for cytotoxicity according to ISO 10993 using L929 fibroblasts. Fig. 8 presents SEM micrographs of L929 cells cultured on silk and PBS textile scaffolds for up to 14 days (Fig. 8A) and the corresponding dsDNA quantification (Fig. 8B).

SEM analysis (Fig. 8A) revealed that at early time points L929 fibroblasts showed good adherence to the SF and PBS structures. The cells seemed to be rounder on the PBS surface, in contrast to cells on the SF scaffolds, which displayed a typical fibroblastic morphology. Despite this, the cells were well able to colonize the structures. After 14 days culture the cells had a characteristic fibroblast morphology on both materials. The methylene blue results (data not shown) confirmed that L929 cells were able to adhere to the surface of PBS and SF scaffolds and proliferate over time. Cell proliferation is represented as the variation with time of the amount of dsDNA in cells adherent on both materials and TCPS. The DNA measurements showed continuous proliferation of L929 cells on the silk scaffolds, but not on the PBS structures. Cells were able to proliferate on the PBS from day 1 to day 7, but the amount of DNA did not vary from day 7 to day 14, as shown in Fig. 8B.

Cells were able to adhere to and o colonize the scaffolds for up to 14 days culture, without apparent detrimental effects due to the material and/or respective leachables. Even considering the temporal limitation of the in vitro tests to draw conclusions regarding the effect of degradation products of the proposed structures, those are considered sufficient to discard the effect of processing additives such as plasticizers in the case of PBS structures, which are expected to leach out within the defined time frame [63]. These results are in agreement with the literature, in which SF (after sericin removal) and PBS scaffolds, processed using other methodologies, have demonstrated a lack of deleterious effects of their degradation products, both in vitro and in vivo [64–67].

Despite the lack of cytotoxic events, L929 behaved differently on the surface of the two structures, justified by the distinct fibre morphologies and surface physico-chemical properties, which directly contribute to cell attachment and proliferation [68]. At early time points the morphology of L929 cells on the surface of the SF scaffolds clearly resembled their characteristic fibroblastic morphology, in contrast to the rounder shape on the PBS surfaces.

The crystalline structure, as well as the different surface chemistry of the silk scaffolds, seem to contribute to these observations. In fact, variations in crystallinity lead to changes in surface roughness on the nanometer length scale, to which cells are extremely sensitive, resulting, for example, in distinct focal adhesion formation and subsequent varied cytoskeleton organization and cell shape [69].

The DNA quantification results demonstrated that cells proliferate faster on PBS structures from days 1 to 7, when a plateau was reached, i.e. no increase in DNA amount was registerered on day 14. It can be speculated that the morphology of the fibres/scaffolds has a significant effect on cell proliferation. Although both the SF and PBS fibres have the same linear density they are structurally different, as their filaments differ in thickness and number. The higher number of filaments for SF scaffolds offers a higher surface area for cellular proliferation. Furthermore, physical wear during the degumming process, added to the faster degradation rate (both hydrolytic and enzymatic) of the SF scaffolds could contribute to facilitate cell migration and consequent steady proliferation within the structure.

These results constitute a first validation of the two biotextiles as viable matrices for tissue engineering prior to the development of more complex approaches. Knitting is an effective processing route adding elasticity to the constructs compared with other woven technologies. This is an important property of structural proteins of the extracellular matrix such as elastin. This highly crosslinked and therefore insoluble protein is an essential element of elastic fibres, giving elasticity to tissues such as lung, skin and arteries [70]. This biopolymer is characterized by a rubber-like elasticity, large extensibility before rupture, reversible deformation without loss of energy and high resilience upon stretching [70]. Resilin is another protein that is found in specialized regions of the insect cuticle and demonstrates extraordinary extensibility and elasticity together with fatigue resistance and resilience [71]. These useful properties have inspired material scientists for many years, for several applications, particularly as biomaterials for tissue engineering and drug delivery applications. Elastomeric polypeptides can be produced in relatively high yields in host cells, such as bacteria, and this type of polymer synthesis provides control over the exact amino acid sequence and polymer length [70,72]. However, these processes are far from being industrialized. Therefore, while the bioengineering processes are still making important forward steps towards improving productivity and reproducibility, there is still room for standard polymer processing technologies. Moreover, both of the proposed polymer fibres exhibit tailorable surface chemistries which have enormous potential for the immobilization of such bioengineered molecules, in a combination strategy for the formation of biomimetic substrates to modulate cell responses.

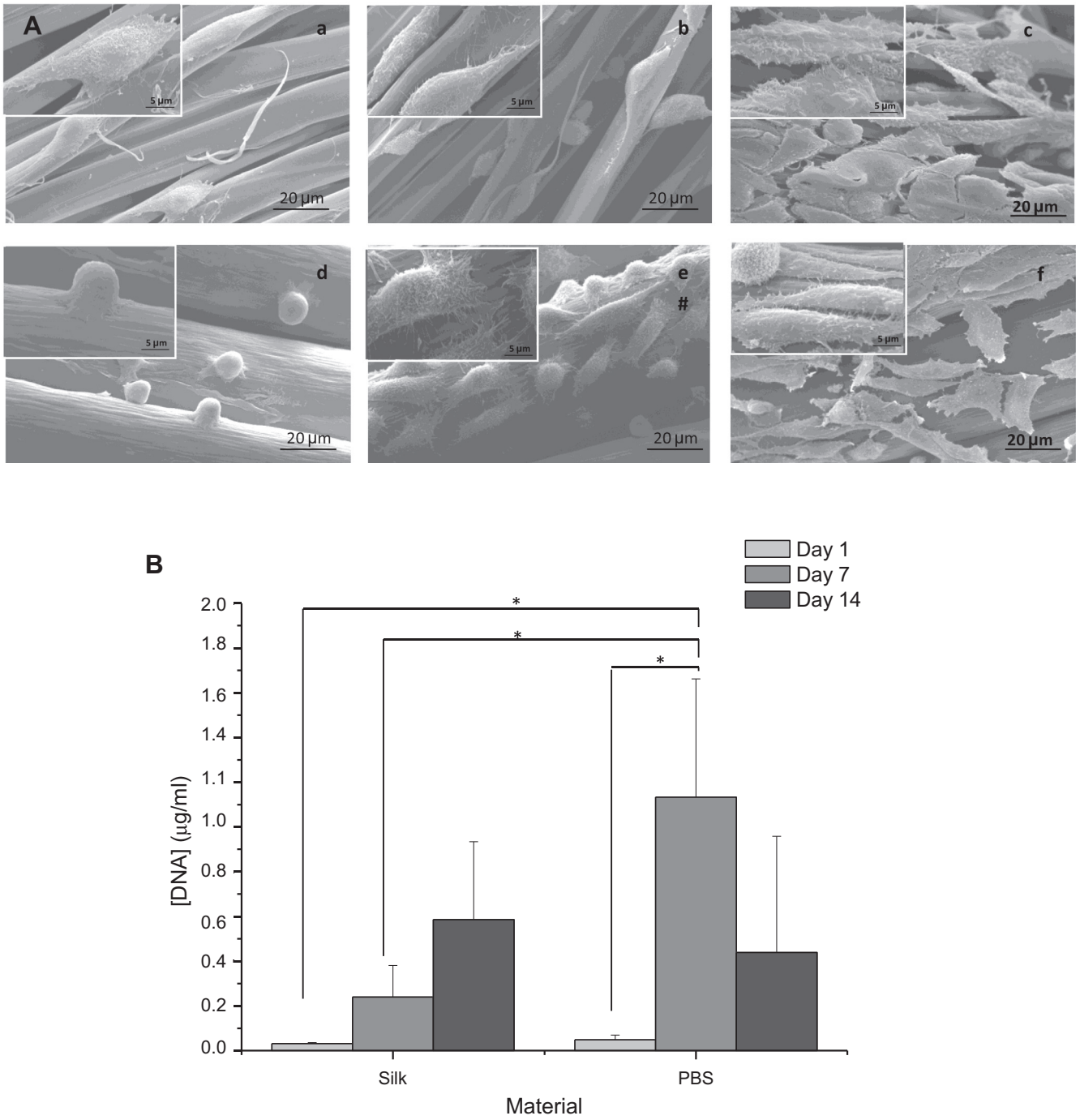


Fig. 8. (A) SEM micrographs of L929 cells cultured on (a–c) silk and (d–f) PBS textile scaffolds for (a, d) 1, (b, e) 7 and (c, f) 14 days. The upper left micrographs represent higher magnification images depicting cell morphological details. (B) Amount of dsDNA, which correlates with the number of L929 cells adherent on the silk and PBS textile scaffolds with time of culture ($^{*}p < 0.05$).

4. Conclusions

Polybutylene succinate has been demonstrated to be a highly processable fibre with excellent performance during knitting. When tested against a SF matrix PBS has been demonstrated to be a very attractive system for tissue engineering applications, with the advantage of having a high level of processing control, from the filament to the final textile structure. On the other hand, although a number of knitted silk structures have been used for several tissue engineering applications the potential of this biotextile is far from being fully explored, which makes our proposed silk-based biotextiles good candidates as rivals to the existing systems. In fact, these two structurally different fibre matrices have mechanical properties, surface chemistries and degradation profiles that can be easily fitted into different tissue engineering scenarios. Moreover, preliminary cellular tests show that the materials can support cell adhesion and proliferation. Finally, the versatility of the weftknitting technology and its reproducibility could open up further industrialization of a tissue engineering product.

Acknowledgements

The authors are grateful to the Portuguese Foundation for Science and Technology (FCT) under the programs POCTI and/or FED-

ER (post-doctoral fellowship to Ana L. Oliveira, SFRH/BPD/39102/2007), and the project TISSUE2TISSUE (PTDC/CTM/105703/2008), founded by FCT agency.

Appendix A. Figure with essential colour discrimination

Certain figure in this article, particularly Fig. 2, is difficult to interpret in black and white. The full colour images can be found in the on-line version, at http://dx.doi.org/10.1016/j.actbio.2013.05.019.

References

[1] King MW, Zhang Z, Guidoin R. Microstructural changes in polyester biotextiles during implantation in humans. J Text Apparel Technol Manage 2001;1:1–8.
[2] Sumanasinghe R, King M. New trends in biotextiles – the challenge of tissue engineering. J Text Apparel Technol Manage 2003;3:1–13.
[3] Moutos FT, Guilak F. Functional properties of cell-seeded three-dimensionally woven poly(epsilon-caprolactone) scaffolds for cartilage tissue engineering. Tissue Eng A 2010;16:1291–301.
[4] Chen X, Qi YY, Wang LL, Yin Z, Yin GL, Zou XH, et al. Ligament regeneration using a knitted silk scaffold combined with collagen matrix. Biomaterials 2008;29:3683–92.
[5] Liu HF, Fan HB, Wang Y, Toh SL, Goh JCH. The interaction between a combined knitted silk scaffold and microporous silk sponge with human mesenchymal stem cells for ligament tissue engineering. Biomaterials 2008;29:662–74.
[6] Fan HB, Liu HF, Toh SL, Goh JCH. Anterior cruciate ligament regeneration using mesenchymal stem cells and silk scaffold in large animal model. Biomaterials 2009;30:4967–77.
[7] Hollister SJ. Scaffold design and manufacturing: from concept to clinic. Adv Mater 2009;21:3330–42.
[8] Salgado AJ, Coutinho OP, Reis RL. Bone tissue engineering: state of the art and future trends. Macromol Biosci 2004;4:743–65.
[9] Tuzlakoglu K, Reis RL. Biodegradable polymeric fiber structures in tissue engineering. Tissue Eng B Rev 2009;15:17–27.
[10] Tao X. Smart fibres, fabrics and clothing. In: Ramakrishna S, editor. Textile scaffolds in tissue engineering. Cambridge: Woodhead Publishing; Cambridge, England: CRC, 2001, 291-313.
[11] Moutos FT, Freed LE, Guilak F. A biomimetic three-dimensional woven composite scaffold for functional tissue engineering of cartilage. Nat Mater 2007;6:162–7.
[12] Ge ZG, Yang F, Goh JCH, Ramakrishna S, Lee EH. Biomaterials and scaffolds for ligament tissue engineering. J Biomed Mater Res A 2006;77A:639–52.
[13] Laurencin CT, Freeman JW. Ligament tissue engineering: an evolutionary materials science approach. Biomaterials 2005;26:7530–6.
[14] Stevens MM, Marini RP, Schaefer D, Aronson J, Langer R, Shastri VP. In vivo engineering of organs: the bone bioreactor. Proc Natl Acad Sci USA 2005;102:11450–5.
[15] Wang XG, Han CM, Hu XL, Sun HF, You CG, Gao CY, et al. Applications of knitted mesh fabrication techniques to scaffolds for tissue engineering and regenerative medicine. J Mech Behav Biomed 2011;4:922–32.
[16] Zou XH, Zhi YL, Chen X, Jin HM, Wang LL, Jiang YZ, et al. Mesenchymal stem cell seeded knitted silk sling for the treatment of stress urinary incontinence. Biomaterials 2010;31:4872–9.
[17] Yagi T, Sato M, Nakazawa Y, Tanaka K, Sata M, Itoh K, et al. Preparation of double-raschel knitted silk vascular grafts and evaluation of short-term function in a rat abdominal aorta. J Artif Org 2011;14:89–99.
[18] Gundy S, Manning G, O'Connell E, Ella V, Harwoko MS, Rochev Y, et al. Human coronary artery smooth muscle cell response to a novel PLA textile/fibrin gel composite scaffold. Acta Biomater 2008;4:1734–44.
[19] Van Lieshout MI, Vaz CM, Rutten MCM, Peters GWM, Baaijens FPT. Electrospinning versus knitting: two scaffolds for tissue engineering of the aortic valve. J Biomat Sci Polym Ed 2006;17:77–89.
[20] Sahoo S, Toh SL, Goh JCH. A bFGF-releasing silk/PLGA-based biohybrid scaffold for ligament/tendon tissue engineering using mesenchymal progenitor cells. Biomaterials 2010;31:2990–8.
[21] Chen JL, Yin Z, Shen WLA, Chen XA, Heng BC, Zou XAH, et al. Efficacy of hESC-MSCs in knitted silk–collagen scaffold for tendon tissue engineering and their roles. Biomaterials 2010;31:9438–51.
[22] Vaquette C, Kahn C, Frochot C, Nouvel C, Six JL, De Isla N, et al. Aligned poly(L-lactic-co-caprolactone) electrospun microfibers and knitted structure: a novel composite scaffold for ligament tissue engineering. J Biomed Mater Res A 2010;94A:1270–82.
[23] Chen GP, Sato T, Ushida T, Hirochika R, Ochiai N, Tateishi T. Regeneration of cartilage tissue by combination of canine chondrocyte and a hybrid mesh scaffold. Mater Sci Eng C: Biol Sci 2004;24:373–8.
[24] Dai WD, Kawazoe N, Lin XT, Dong J, Chen GP. The influence of structural design of PLGA/collagen hybrid scaffolds in cartilage tissue engineering. Biomaterials 2010;31:2141–52.
[25] Kawazoe N, Inoue C, Tateishi T, Chen GP. A Cell Leakproof PLGA–collagen hybrid scaffold for cartilage tissue engineering. Biotechnol Progr 2010;26:819–26.
[26] Ng KW, Khor HL, Hutmacher DW. In vitro characterization of natural and synthetic dermal matrices cultured with human dermal fibroblasts. Biomaterials 2004;25:2807–18.
[27] Lyoo WS, Kim JH, Yoon WS, Ji BC, Choi JH, Cho J, et al. Effects of polymer concentration and zone drawing on the structure and properties of biodegradable poly(butylene succinate) film. Polymer 2000;41:9055–62.
[28] Li H, Chang J, Cao A, Wang J. In vitro evaluation of biodegradable poly(butylene succinate) as a novel biomaterial. Macromol Biosci 2005;5:433–40.
[29] Oliveira JT, Correlo VM, Sol PC, Costa-Pinto AR, Malafaya PB, Salgado AJ, et al. Assessment of the suitability of chitosan/polybutylene succinate scaffolds seeded with mouse mesenchymal progenitor cells for a cartilage tissue engineering approach. Tissue Eng A 2008;14:1651–61.
[30] Correlo VM, Boesel LF, Bhattacharya M, Mano JF, Neves NM, Reis RL. Properties of melt processed chitosan and aliphatic polyester blends. Mater Sci Eng A: Struct 2005;403:57–68.
[31] Correlo VM, Costa-Pinto AR, Sol P, Covas JA, Bhattacharya M, Neves NM, et al. Melt processing of chitosan-based fibers and fiber-mesh scaffolds for the engineering of connective tissues. Macromol Biosci 2010;10:1495–504.
[32] Altman GH, Diaz F, Jakuba C, Calabro T, Horan RL, Chen J, et al. Silk-based biomaterials. Biomaterials 2003;24:401–16.
[33] Horan RL, Collette AL, Lee C, Antle K, Chen J, Altman GH. Yarn design for functional tissue engineering. J Biomech 2006;39:2232–40.
[34] Kim U-J, Park J, Joo Kim H, Wada M, Kaplan DL. Three-dimensional aqueous-derived biomaterial scaffolds from silk fibroin. Biomaterials 2005;26:2775–85.
[35] Oliveira AL, Sun L, Kim HJ, Hu X, Rice W, Kluge J, et al. Aligned silk-based 3-D architectures for contact guidance in tissue engineering. Acta Biomater 2012;8:1530–42.
[36] Chen, J., Altman, G., Horan, R., Horan, D. Immunoneutral silk-fiber-based medical devices (2012). European Patent No. EP 2426241. Munich, Germany: European Patent Office.
[37] Shalaby SW, Peniston S, Carpenter KA. Selectively absorbable/biodegradable, fibrous composite constructs and applications thereof. WIPO Patent No. 2008069915, Geneva, Switzerland, 2008.
[38] Shalaby SW. Silk/absorbable polyester hybrid medical devices and applications thereof. US Patent 20,080,103,525, issued May 1, 2008.
[39] Gravett DM, Signore PE, Wang K, Toleikis PM, Guan D, Hu Z, et al. Silk stent grafts. US Patent Application 10/748,747, 2003.
[40] Altman GH, Horan RL, Lu HH, Moreau J, Martin I, Richmond JC, et al. Silk matrix for tissue engineered anterior cruciate ligaments. Biomaterials 2002;23:4131–41.
[41] Yan L-P, Oliveira JM, Oliveira AL, Caridade SG, Mano JF, Reis RL. Macro/microporous silk fibroin scaffolds with potential for articular cartilage and meniscus tissue engineering applications. Acta Biomater 2012;8:289–301.
[42] Lu Q, Zhu HS, Zhang CC, Zhang F, Zhang B, Kaplan DL. Silk self-assembly mechanisms and control from thermodynamics to kinetics. Biomacromolecules 2012;13:826–32.
[43] Owens DK, Wendt RC. Estimation of the surface free energy of polymers. J Appl Polym Sci 1969;13:1741–7.
[44] Kaelble DH. Dispersion-polar surface tension properties of organic solids. J Adhesion 1970;2:66–81.
[45] Taniguchi I, Nakano S, Nakamura T, El-Salmawy A, Miyamoto M, Kimura Y. Mechanism of enzymatic hydrolysis of poly(butylene succinate) and poly(butylene succinate-co-L-lactate) with a lipase from *Pseudomonas cepacia*. Macromol Biosci 2002;2:447–55.
[46] Horan RL, Antle K, Collette AL, Wang Y, Huang J, Moreau JE, et al. In vitro degradation of silk fibroin. Biomaterials 2005;26:3385–93.
[47] Van Krevelen DW. Properties of polymers. Amsterdam: Elsevier; 1990.
[48] Yoo ES, Im SS. Melting behavior of poly(butylene succinate) during heating scan by DSC. J Polym Sci B: Polym Phys 1999;37:1357–66.
[49] Hutmacher DW, Schantz JT, Lam CXF, Tan KC, Lim TC. State of the art and future directions of scaffold-based bone engineering from a biomaterials perspective. J Tissue Eng Regener Med 2007;1:245–60.
[50] O'Brien FJ, Harley B, Yannas IV, Gibson LJ. The effect of pore size on cell adhesion in collagen–GAG scaffolds. Biomaterials 2005;26:433–41.
[51] Williams JL, Lewis JL. Properties and an anisotropic model of cancellous bone from the proximal tibial epiphysis. J Biomech Eng T ASME 1982;104:50–6.
[52] Altman GH, Diaz F, Jakuba C, Calabro T, Horan RL, Chen JS, et al. Silk-based biomaterials. Biomaterials 2003;24:401–16.
[53] Perez-Rigueiro J, Viney C, Llorca J, Elices M. Mechanical properties of silkworm silk in liquid media. Polymer 2000;41:8433–9.
[54] Coutinho DF, Pashkuleva IH, Alves CM, Marques AP, Neves NM, Reis RL. The effect of chitosan on the in vitro biological performance of chitosan–poly(butylene succinate) blends. Biomacromolecules 2008;9:1139–45.
[55] Martins A, Gang W, Pinho ED, Rebollar E, Chiussi S, Reis RL, et al. Surface modification of a biodegradable composite by UV laser ablation: in vitro biological performance. J Tissue Eng Regener Med 2010;4:444–53.
[56] Arai T, Freddi G, Innocenti R, Tsukada M. Biodegradation of *Bombyx mori* silk fibroin fibers and films. J Appl Polym Sci 2004;91:2383–90.
[57] Israelachvili JN, Mcguiggan PM. Forces between surfaces in liquids. Science 1988;241:795–800.
[58] Horan RL, Antle K, Collette AL, Huang YZ, Huang J, Moreau JE, et al. In vitro degradation of silk fibroin. Biomaterials 2005;26:3385–93.
[59] Varma IK, Albertsson A-C, Rajkhowa R, Srivastava RK. Enzyme catalyzed synthesis of polyesters. Prog Polym Sci 2005;30:949–81.
[60] West JL, Hubbell JA. Polymeric biomaterials with degradation sites for proteases involved in cell migration. Macromolecules 1999;32:241–4.

[61] Li M, Ogiso M, Minoura N. Enzymatic degradation behavior of porous silk fibroin sheets. Biomaterials 2003;24:357–65.
[62] Wang M, Jin HJ, Kaplan DL, Rutledge GC. Mechanical properties of electrospun silk fibers. Macromolecules 2004;37:6856–64.
[63] ANSI/AAMI/ISO. Standard 10993–5. Biological evaluation of medical devices: tests for cytotoxicity, in vitro methods.: Association for the Advancement of Medical Instrumentation; Geneva, Switzerland, 1999.
[64] Meinel L, Hofmann S, Karageorgiou V, Kirker-Head C, McCool J, Gronowicz G, et al. The inflammatory responses to silk films in vitro and in vivo. Biomaterials 2005;26:147–55.
[65] Zhou JA, Cao CB, Ma XL, Hu L, Chen LA, Wang CR. In vitro and in vivo degradation behavior of aqueous-derived electrospun silk fibroin scaffolds. Polym Degrad Stab 2010;95:1679–85.
[66] Costa-Pinto AR, Correlo VM, Sol PC, Bhattacharya M, Srouji S, Livne E, et al. Chitosan–poly(butylene succinate) scaffolds and human bone marrow stromal cells induce bone repair in a mouse calvaria model. J Tissue Eng Regener Med 2012;6:21–8.
[67] Correlo VM, Pinho ED, Pashkuleva I, Bhattacharya M, Neves NM, Reis RL. Water absorption and degradation characteristics of chitosan-based polyesters and hydroxyapatite composites. Macromol Biosci 2007;7:354–63.
[68] Alves NM, Pashkuleva I, Reis RL, Mano JF. Controlling cell behavior through the design of polymer surfaces. Small 2010;6:2208–20.
[69] Washburn NR, Yamada KM, Simon Jr CG, Kennedy SB, Amis EJ. High-throughput investigation of osteoblast response to polymer crystallinity: influence of nanometer-scale roughness on proliferation. Biomaterials 2004;25:1215–24.
[70] van Eldijk MB, McGann CL, Kiick KL, van Hest JC. Elastomeric polypeptides. Top Curr Chem 2012;310:71–116.
[71] Qin G, Hu X, Cebe P, Kaplan DL. Mechanism of resilin elasticity. Nat Commun 2012;3:1003.
[72] Xia XX, Xu QB, Hu X, Qin GK, Kaplan DL. Tunable self-assembly of genetically engineered silk-elastin-like protein polymers. Biomacromolecules 2011;12:3844–50.